Prediction of Motion Sickness Onset for Vertical Lift Applications

Philippe J. Petit*
Research Engineer
German Aerospace Center (DLR), Brunswick, Germany

It is foreseen that in the upcoming application of (electric) urban air taxis, the comfort of ride and especially the experience of motion sickness will play a vital role in acceptance among passengers and therefore economic success of these vehicles. For this reason, accurate motion sickness prediction models are needed, which later can be employed for, for example, kinetosis-low trajectory generation. Established motion sickness models like the ISO 2631 standard, however, only take into account the vertical translational axis and no rotational axis. For this reason, the 6-degrees-of-freedom Kamiji motion sickness model is selected and modified in order to circumvent unsatisfactory prediction results with this model. Subsequently, the parameters of this model are retuned by employing an optimization approach based on published experimental data. It is then shown that with this approach, the modified Kamiji model is better suited for predicting the motion sickness results of this dataset. In the future, this model shall be tested and validated via a series of flight tests with test subjects in DLR's BO-105 helicopter.

Nomenclature

a	acceleration vector, m/s^2
b	Hill function parameter
c	motion conflict
f	resultant otholite force
g	gravity vector, m/s^2
h	Hill function output
K_a	acceleration gain
K_{ac}	feedback gain acceleration conflict
K_{out}	output gain
K_{vc}	feedback gain sensed vertical
K_ω	rotational rates gain
$K_{\omega c}$	feedback gain rotational rates conflict
p	Kamiji parameter vector
$\mathbf{R}_{\text{HI}}$	rotational matrix head to an inertial frame
s	Laplace-transform variable
t_{end}	simulation end time
v	sensed vertical
x	motion parameter setting
z	Z-transform variable
Δ	difference
τ	subjective vertical time, s constant, s
τ_a	semicircular canals (SCC) time constant, s
τ_d	SCC time constant, s
φ	roll angle, rad
ω	rotational velocities vector, rad/s
$\square_{\text{Griffin}}$	Griffin dataset
$\square_I$	inertial frame
$\square_{\text{lb}}$	lower bound
$\square_{\text{sim}}$	simulated data
$\square_{\text{ub}}$	upper bound
$\hat{\square}$	estimated value
$\tilde{\square}$	head internal value
$\hat{\tilde{\square}}$	estimated head internal value

Introduction

Motion sickness, also known as kinetosis, can be induced by various means. These include railway travel (Ref. 1), ship travel (Ref. 2), car travel (Ref. 3), air travel (Ref. 4), and motion simulators (Ref. 5). Symptoms include nausea, vomiting, cold sweat, headache, sleepiness, yawning, loss of appetite, and increased salivation, which also convey the idea that kinetosis is an important factor for crew comfort in air transport applications.

It has been identified that kinetosis is a noteworthy topic for some forms of transport, most prominently perhaps, railway transport where the introduction of tilting trains promoted the study of this topic. Especially in countries where high-speed trains are introduced to curvy tracks, motion sickness becomes a problem among passengers (Ref. 1).

It can be easily seen that a similar problem arises for more modern transport solutions such as self-driving carsickness as dubbed by Diels and Bos in Ref. 6. If we extrapolate these arguments for the upcoming technology of urban air transport as proposed by numerous startups and companies, it is easily imaginable that motion sickness poses a serious problem for this kind of transport, especially if considering the

*Corresponding author; email: philippe.petit@dlr.de.
Presented at the VFS Annual Forum, Virtual, May 10–14, 2021. Manuscript received September 2021; accepted October 2022.

proposed air taxis, which will most likely travel at low altitude over dense urban airspace in conjuncture with many other air taxis. Such operating conditions will not only generate fairly complex movement patterns but are also prone to atmospheric disturbances like gusts. Given these circumstances, it is predicted that motion sickness will play a substantial role in the adoption of such urban air mobility concepts and therefore also in the ultimate economic success of these solutions. People certainly will not be excited about a transport solution which is faster but makes them sick every time it is used.

This argument raises the following research question: How can kinetosis be accurately predicted given a flight path or an aircraft motion of for example, a vertical takeoff and landing urban air taxi? If an accurate prediction model for kinetosis can be formulated, subsequent design steps for for example, flight controllers or improved trajectory layout can be achieved in future work. For this, however, a prediction model taking into account the six degrees of freedom (DoF) of an aircraft is mandatory which can cope with as arbitrary inputs as possible.

Kinetosis models

The ISO 2631-1 (Ref. 7) is probably the most established standard to judge the occurrence of kinetosis due to the vibration of the human body. For this, the standard specifies the motion sickness dose value ($MSDV_z$) which is calculated via the root-mean-square value of a given frequency-weighted vertical acceleration. Other metrics for the calculation of kinetosis occurrence are the ADS-27-A-SP, specifically for helicopters, or the NASA ride quality index. However, Rath and Fichter (Ref. 8) showed that the ISO 2631 is the most general case and implicitly includes the other two methods.

While the ISO-2631 is simple and in widespread use, it only applies to vertical acceleration. This shortcoming becomes evident when the ISO-2631 approach is applied to more complicated motions like that of an aircraft. Turner et al. (Ref. 4) showed that the kinetosis incidence rate cannot be explained with simple linear accelerations alone. Considerable research effort has been performed in order to find similar frequency weightings or metrics for other axes including lateral acceleration, rolling motion, and combined vibration by Griffin et al. (Refs. 9–11). However, this research has not culminated in an applicable weighting or metric.

Another approach hinges on the direct modeling of the kinetosis mechanism. Perhaps the most accepted theory for this mechanism is the "conflict theory" by Reason and Brand (Ref. 12), which postulates that motion sickness arises from conflicting motion perceptions by the inner ear and the eyes. This discrepancy is then interpreted by the brain such that the subject experiences the typical motion sickness syndromes like illness, stomach awareness, and so on. Based on the conflict theory, Bos and Bles (Ref. 13) developed a model which directly simulated this conflict by numerical simulation, parameterized by experimental values. For simplicity, this model, however, was only developed in one dimension. Building on this idea, Kamiji et al. (Ref. 14) expanded this simulation model to six axes including three rotational and three translational DoF. This expansion makes the Kamiji model suitable for the application on aircraft. The model, therefore, offers a new way of interpreting empirical data of, for example, short-haul flights (Ref. 4). However while this model offers the flexibility to assess arbitrary motions, it still lacks sufficient accuracy as can be seen by comparing the output of the Kamiji model and that of empirical data.

In an attempt to gain a high-fidelity model, which also offers accurate motion sickness prediction, empirical data gained from a set of papers published by Griffin et al. will be used in the following in order to tune the parameters of a modified Kamiji model, therefore gaining a better suited 6-DoF motion sickness model.

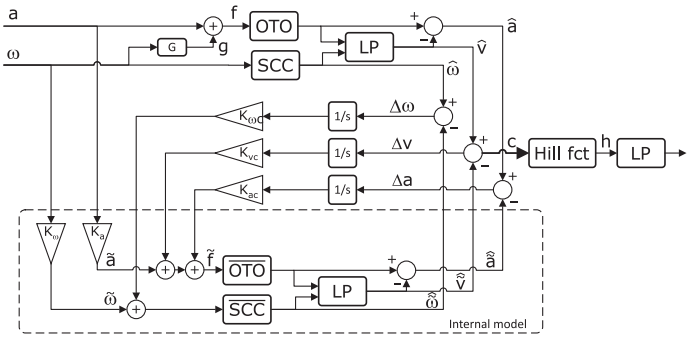

Fig. 1. The block diagram of the original Kamiji kinetosis model.

Kamiji Kinetosis Model

The motion sickness conflict theory postulates that motion sickness arises from a conflict or mismatch between the physical vestibular system consisting of the semicircular canals (SCC) as well as the otoliths (OTO) and the "internal mode" brain replica of these two blocks $\overline{SCC}$ and $\overline{OTO}$ (Refs. 12, 13). While the physical vestibular system senses rotational rates via the SCC and translational acceleration via the OTO analogous to gyroscopes and accelerometers in modern inertial measurement units, the inner model of the vestibular system bases its output on the visual input of the eyes, thereby estimating what the rotational rates and translational acceleration *should be*, given the current optical impression. The conflict or mismatch of these two motion estimations is what is causing motion sickness according to the conflict theory.

The original Kamiji kinetosis model, which is depicted in Fig. 1, hinges on the idea of directly modeling this theory. This model therefore implements the physical vestibular system consisting of the SCC as well as the OTO, which are modeled in the top half of the model and the "internal mode" marked by $\overline{SCC}$ and $\overline{OTO}$ which is also explicitly modeled in the lower half. Inputs to the model are three-dimensional (3D) vectors for rotational rates and translational accelerations. The output of both vestibular systems is subtracted and forms the motion conflict c. In order to accumulate this signal, it is fed into the "Hill function," which acts as a signal range converter and together with an integrating second-order low-pass filter produces the motion sickness incidence (MSI). The Hill function defined by Eq. 1 accumulates the motion conflict c to asymptotically form a number between 0 and 1. The main idea is that people cannot get "sicker than sick," which motivates the choice for an asymptotical function (Ref. 13). An example output for $n = 2$ and $b = 0.5$ is depicted in Fig. 2.

$$h = \frac{(c/b)^n}{1 + (c/b)^n} \tag{1}$$

Both the physical otholite system OTO as well as the internal model of the otholites $\overline{OTO}$ are modeled as unit matrices. The SCC are modeled as

$$\hat{\omega}_i = \frac{\tau_d \tau_a s^2}{(\tau_d s + 1)(\tau_a s + 1)} \cdot \omega_i \qquad (i = x, y, z) \tag{2}$$

While its internal counterpart $\overline{SCC}$ is modeled as (Ref. 14)

$$\hat{\tilde{\omega}}_i = \frac{\tau_d s}{\tau_d s + 1} \tilde{\omega}_i \qquad (i = x, y, z) \tag{3}$$

The block denoted as G generates the earth's gravitational acceleration, which is rotated via the inertial rotational rate as given by

$$\frac{d\mathbf{g}}{dt} = -\omega \times g. \tag{4}$$

The total acceleration acting on the otholites is formed as $f = g + a$.

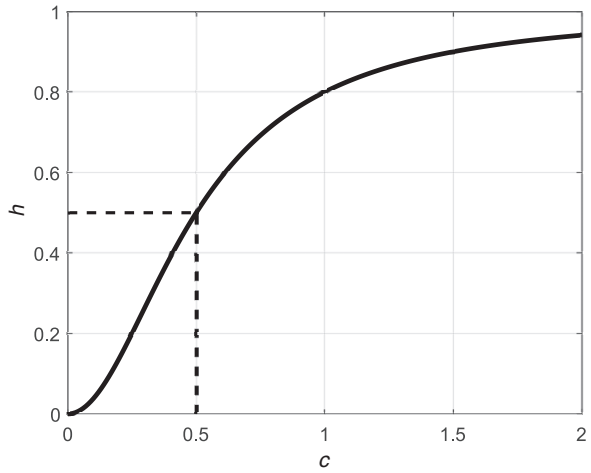

Fig. 2. Hill function visualization for $n = 2$ and $b = 0.5$.

Table 1. Motion sickness scale used by Griffin et al.

0	No symptoms
1	Any symptoms, however slight
2	Mild symptoms
3	Mild nausea
4	Mild to moderate nausea
5	Moderate nausea but can continue
6	Moderate nausea and want to stop

The gains $K_{\omega C}$, K_{VC}, and K_{aC} are feedback gains for the differences in estimated acceleration, rotational rate, and subjective vertical, respectively.

Kamiji et al. defined the coordinate with its origin in the center of the head, such that the x-axis was pointing forward, the y-axis pointing sideward to the left, and the z-axis orthogonal to the x- and y-axes pointing upward. The input vectors a and ω are represent quantities in this "head" coordinate system. For further information regarding this model, refer to the original publication (Ref. 14).

Griffin Papers Dataset

The authors Donohew, Joseph, and Beard published a total of five different papers (Ref. 9–11, 15, 16), which contained empirical data and analysis of motion sickness experiments which were conducted with humans in order to better understand the effects of different motion forms on motion sickness. For the various studies, different motion conditions were generated with the help of the 12-m Tilting and Translating Cabin setup of the Institute of Sound and Vibration Research, University of Southampton. In every test, a human test subject rode inside this cabin while periodically filling out a motion sickness questionnaire. The tests involved horizontal lateral translational acceleration with or without simultaneous tilting of the cabin. The frequencies of the generated motions ranged from 0.0315 to 0.8 Hz. Due to the harmonic nature of the oscillation, jerk, acceleration, velocity, and displacement are physically linked. However, the limits of these values are naturally dictated by the limit of the motion generator. The limits of this particular 12-m Tilting and Translating Cabin are displayed in Fig. 3 and are taken from Ref. 10. As all tests were conducted such that the simulator was performing at its limits, frequency is directly linked to maximal jerk, acceleration, velocity, and displacement via the envelope bound of the simulator. The displacement limits can be summarized as given by Eq. 5.

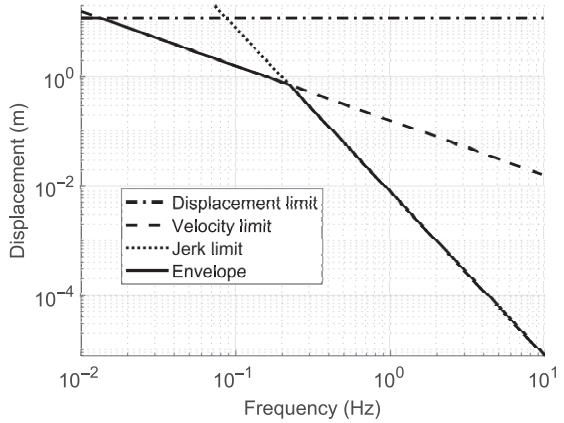

Fig. 3. Displacement Limits of the 12-m Tilting and Translating Cabin of the University of Southampton.

$$D(f) = \begin{cases} 12 & f \leq 0.013 \text{ Hz} \\ 12 \cdot 1 \cdot \frac{1}{2\pi f} & 0.01328 \text{ Hz} < f < 0.223 \text{ Hz} \\ 12 \cdot 1.96 \cdot \frac{1}{2\pi f} & 0.223 \text{ Hz} \leq f \end{cases} \quad (5)$$

In total this dataset consists of 560 subjects completing a total of 620 h of testing inside the motion simulator. The setup of the different tests was remarkably similar over the various papers: each subject completed 30 min of exposure to one motion candidate while rating the subjective motion sickness every minute on a scale from 0 (no symptoms) to 6 (moderate nausea and want to stop) as listed in Table 1. During the tests, the subjects sat inside the cabin lit by a 40-W light bulb with headphones emitting white noise. No external view was given to the subjects.

In total, 31 motion test points, each consisting of one motion candidate which was tested on 20 subjects and its capability of provoking motion sickness, were extracted from the aforementioned papers and parsed into a unified dataset. The parameters of motions that were tested across the different papers are visualized in Fig. 4. Some points were tested several times across papers, which is why some points coincide in Fig. 4.

It should be noted that the rolling motion was parameterized by % compensation, which denotes to which degree the cabin was tilted in order to compensate for lateral acceleration such that the acceleration felt by the subject would still be vertical. This was done in order to emulate a railway vehicle "leaning" or "tilting" into a curve. In aerospace terms, this would be the equivalent of a coordinated turn. For example, a 100% compensation would mean that the cabin was tilted exactly so that the test subject does not feel any lateral acceleration, but only an oscillating, slightly higher vertical acceleration. On the other hand, 0% compensation would mean that the cabin would be accelerated laterally without any tilting (rolling) of the cabin.

$$\phi(t) = -\arctan\left(c \cdot \frac{a_y(t)}{g}\right) \quad (6)$$

This relation can be mathematically expressed by correlating the tilt angle ϕ with the earth acceleration g, the compensation c ranging from 0 to 1, and the lateral acceleration a_y via Eq. 6. The coordinate system is shown in Fig. 5. As at the time, all authors were members of the group of Prof. Griffin, this dataset will be referred to as the "Griffin dataset" in the following.

While this research was originally intended for general motion sickness research with a focus on railway applications, the Griffin dataset

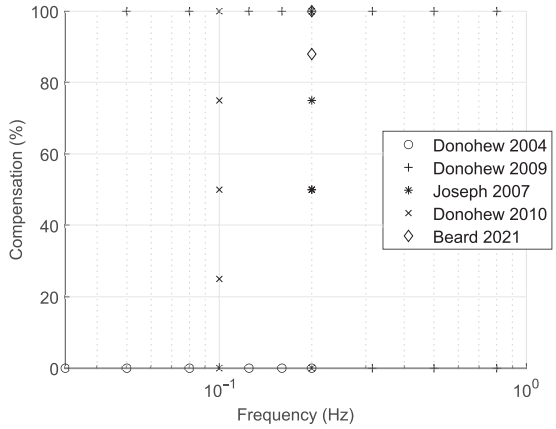

Fig. 4. Motion parameter space covered during experiments performed in Refs. 9–11, 15, and 16 for determining motion sickness of motion. Each point was tested with at least 20 test subjects.

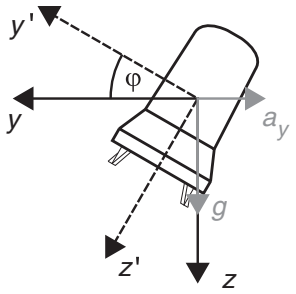

Fig. 5. The coordinate system used for describing the lateral acceleration compensation.

is after all a good fit for the purpose of this study. It offers reliable high-quality data with a consistent experiment setup with a high number of test candidates. Additionally, the data entail horizontal motions with combined roll motion closely mimicking coordinated turns in horizontal flight. The downside of this dataset compared to a dedicated dataset tailored towards aerospace applications is the limited range of motion of the employed motion simulator as well as the fact that the test subjects had no external view during testing. Also, this dataset does not include vertical oscillations which, although to a lesser degree than horizontal turns, still play a major role in vertical lift applications. However, considering the extent of the data and the effort it would cost to reproduce such data, the Griffin dataset is well suited for tuning a motion sickness model intended for vertical lift aerial transport applications.

Optimization

The goal of the optimization is to determine an improved set of parameters for the Kamiji model. These shall then be tuned such that they predict the same motion sickness values as observed during the experiment when the motions of that experiment are handed to the model. In order to achieve this, a numerical optimization approach will be leveraged, which attempts to minimize the difference between the motion sickness level as predicted by the model and that observed during the tests. First, the employed optimization approach will be presented, followed by the introduction of a modified Kamiji model which shall improve the suitability for optimization.

Computation of optimization

The goal of the optimization problem is to find the optimal set of parameters $\vec{p}^*$ with which the results of the simulation $\vec{y}_{\text{sim}}(\vec{p}^*)$ most closely match with those of the Griffin dataset $\vec{y}_{\text{Griffin}}$. The optimization problem is formally described as

$$\min_{\vec{p}} \quad \|\vec{y}_{\text{sim}}(\vec{p}) - \vec{y}_{\text{Griffin}}\|_2 \tag{7a}$$

$$\text{subject to} \quad \vec{p} \geq \vec{p}_{\text{lb}}, \tag{7b}$$

$$\vec{p} \leq \vec{p}_{\text{ub}} \tag{7c}$$

with the subscripts $_{\text{Griffin}}$ and $_{\text{sim}}$ each mark that the data stem from the Griffin dataset or from simulated data using the modified Kamiji simulation which will be introduced in the next section. The model parameters of the blocks described in Eqs. (1)–(3) as well as the various gains of the model are structured in a single parameter vector described by

$$\vec{p} = (K_a \;\; K_{\text{ac}} \;\; K_\omega \;\; K_{\omega c} \;\; K_{\text{vc}} \;\; \tau \;\; \tau_a \;\; \tau_d \;\; K_{\text{out}})^\intercal. \tag{8}$$

Additionally, the motion parameters (frequency, % compensation, amplitude, etc.) of the Griffin dataset are organized in the vector $\vec{x}$. The dataset consists of 31 discrete sets of motion parameters, which are indicated by the subscript $_i$ with i denoting the ith dataset. The final MSI value for each of the 31 motion sets for the simulated and experimental results is structured in two vectors:

$$\vec{y}_{\text{sim}}(\vec{p}) = (MSI_{\text{sim}}(\vec{p}, \vec{x}_1, t_{\text{end}}), \;\; MSI_{\text{sim}}(\vec{p}, \vec{x}_2, t_{\text{end}}), \;\; \ldots, \;\; MSI_{\text{sim}}(\vec{p}, \vec{x}_{31}, t_{\text{end}}))^\intercal \tag{9}$$

$$\vec{y}_{\text{Griffin}} = (MSI_{\text{Griffin}}(\vec{x}_1, t_{\text{end}}), \;\; MSI_{\text{Griffin}}(\vec{x}_2, t_{\text{end}}), \;\; \ldots, \;\; MSI_{\text{Griffin}}(\vec{x}_{31}, t_{\text{end}}))^\intercal. \tag{10}$$

Hereby the vector specifying the motion conditions such as % compensation, motion frequency f, motion sickness scale, etc., will be denoted as $\vec{x}_i$, being the ith motion setting.

The Griffin dataset specifies the percentage of people reaching each of the motion sickness levels specified in Table 1; therefore, in total six different vectors $\vec{y}_{\text{Griffin}}$ exist. This in turn leads to six different optimizations each resulting in a different set of parameters $\vec{p}$ for each of the motion sickness levels. This means that given a specific motion one of the six different motion sickness models can be used to predict motion sickness. For example, if the motion sickness model level 4 is applied, that model predicts the percentage of people reaching level 4 *or higher*. This approach was chosen as the Griffin dataset contains less and less information at a higher motion sickness level. This fact will be further explained in the Results section of this paper.

For the sake of verification, implementation speed, and traceability, the modified Kamiji model was first implemented using MATLAB/Simulink™. However due to long invocation and compilation time of Simulink, the Simulink model could not be used directly for the optimization. For this reason, the model was rewritten as an ODE executed by a suitable MATLAB™ ODE solver in the MATLAB™ programming language. The model was subsequently autocoded to a *.mex* file, which significantly decreased simulation and therefore overall execution time of the optimization.

The simulation model itself was set up such that it reflected the Griffin papers as detailed above; therefore, the simulation time was set to $t_{\text{end}} = 30$ min, with the motion mirroring those of the specific motion candidate. For the optimization process, MATLAB™'s constrained nonlinear multivariable optimization function *lsqnonlin* was chosen.

The limits in Eqs. (7b) and (7c) have been chosen to roughly match the values as described by Bos and Bles (Ref. 13) as well as Kamiji

Table 2. The chosen upper and lower parameter vector bounds for $\vec{p}$

	K_a	K_{ac}	K_ω	$K_{\omega c}$	K_{vc}	τ	τ_a	τ_d	K_{out}
ub	2	10	10	10	10	20	500	20	100
lb	0.01	0.1	0.1	0.1	0.1	0.1	1	0.1	0.5

et al. (Ref. 14) and to set reasonable bounds for the optimization algorithm without sacrificing too much of the design aspects of the original model. The chosen limits for the parameter vector $\vec{p}$ are listed in Table 2.

Initial optimization results indicated that the optimization tended to overamplify high frequencies. One of the root causes for this problem was identified as being the inherent coupling of the frequency with the acceleration amplitude of the Griffin dataset. The limits of the simulator are set such that experiments conducted at approximately 0.223 Hz experienced the highest acceleration with an acceleration of around 1 m/s^2 Root Mean Square (RMS), while accelerations with lower and higher frequencies fall linearly with frequency as can be seen in Fig. 3. For this reason, additional three "virtual" test points with 0% symptoms were handed to the optimization algorithm. These were placed at a frequency of 1.5 Hz with a compensation of 100% and acceleration values corresponding to 1, 1.5, and 2 m/s^2 RMS oscillations, therefore enforcing high-frequency roll-off.

Modifications for optimization

As a preliminary step for the subsequent optimization of the Kamiji model with the Griffin dataset, some modifications to the original model will be introduced in this paragraph. The modified Kamiji model is depicted in Fig. 6. The added blocks are marked by a dashed line. The main goal of the performed modification was to improve the optimization result and to adapt it to common aerospace standards. A list of modifications is given below:

1) *Introduction of low-pass filters*: While the ISO 2631 details that frequencies provoking motion sickness lie in the range of 0.1–0.5 Hz (Ref. 7), most newer publications broaden this interval with the higher boundary being roughly at 1 Hz. However during the initial assessment the Kamiji model showed insufficient roll-off at frequencies above 1 Hz. In order to correct this behavior, a simple second-order low-pass filter with a conservatively placed cutoff frequency of 4 Hz was introduced in the signal paths leading to the model. The transfer function for this filter is given by

$$LP = \frac{1}{0.0638s^2 + 0.3573s + 1}. \tag{11}$$

These low-pass filters are marked as LP in Fig. 6.

2) *Replacement of the "G" block*: This block is intended to rotate the gravity as well as the acceleration vector into the headframe. In order to assure congruence between the gravity vector and the external acceleration, this transformation is now explicitly stated as

$$\vec{g}_H = \mathbf{R}_{\mathrm{HI}} \cdot \vec{g}_I \tag{12}$$

whereby subscript $_I$ denotes the inertial frame, the subscript $_H$ the headframe and the matrix $\mathbf{R}_{\mathrm{HI}}$ the rotation matrix from the inertial to the headframe. Note that the rotational rates are defined to be also measured in the headframe.

3) *Additional gain K_{out} at the MSI output*: Initial optimization results indicated that depending on the selected kinetosis rating defined by the Griffin paper set given in Table 1, the predicted kinetosis level could not be matched. For this reason, the gain K_{out} was introduced to the output of the modified Kamiji model. This way the optimizer can increase the model's output magnitude for a given motion candidate. However, it is important to notice that one of the properties of the Hill function, namely that the output can never exceed 100%, is broken by this modification.

Results

As described above, in total six different motion sickness prediction models, one for each motion sickness level of Table 1, were generated. The majority of literature on the subject, however, uses the MSI metric introduced by O'Hanlon and and McCauley (Ref. 17), which was pragmatically defined to be the percentage of people vomiting given a certain condition. Studies using MSI include the aforementioned motion

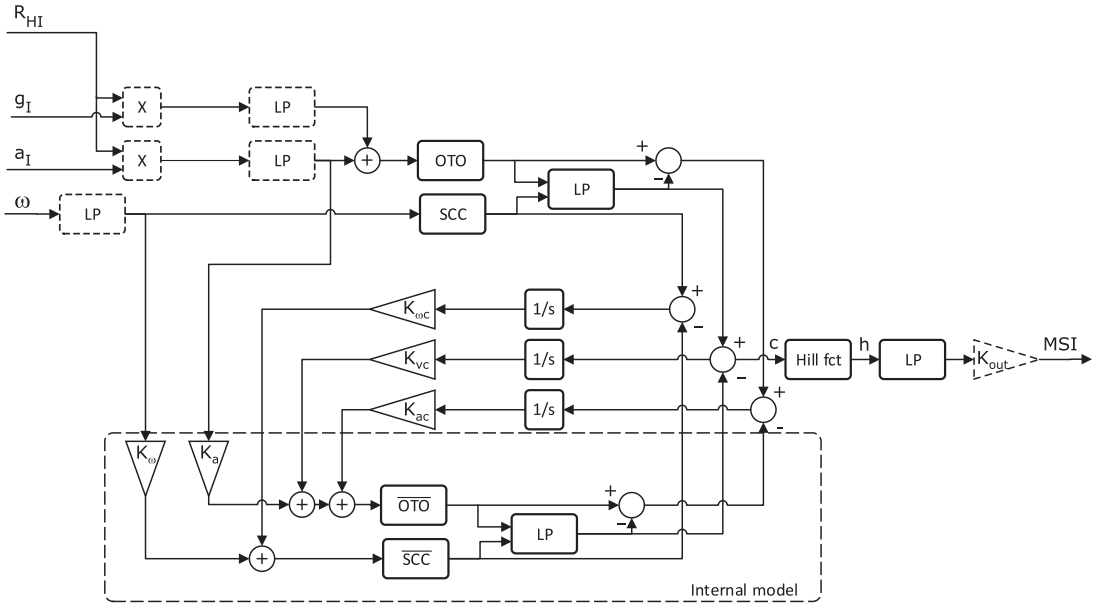

Fig. 6. The block diagram of the modified Kamiji kinetosis model. Newly added blocks are marked with a dashed (- - - - - -) line.

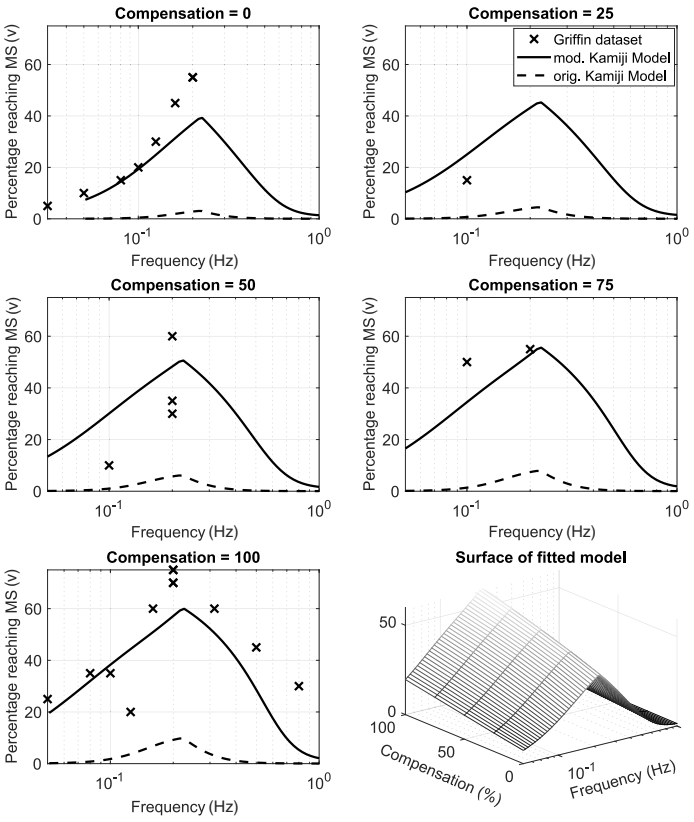

Fig. 7. Percentage of population reaching motion sickness level 3, empirical points of the Griffin dataset in comparison to the original and modified Kamiji model.

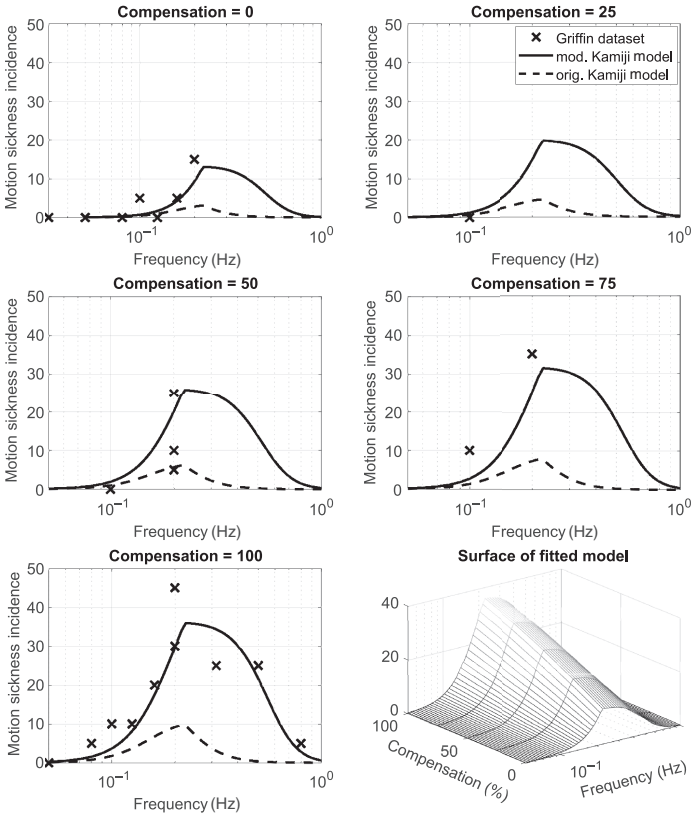

Fig. 8. Percentage of population reaching motion sickness level 6, empirical points of the Griffin dataset in comparison to the original and modified Kamiji model.

sickness models by Kamiji et al. (Ref. 14), the motion sickness model developed by Bos and Bles (Ref. 13) and also the vertical oscillation model of the ISO-2631 (Ref. 7). The definition of MSI is equivalent to the Griffin motion sickness scale level 6. Donohew and Griffin (Ref. 15), on the other hand, used motion sickness level 3 for fitting a motion sickness model for lateral acceleration as this level offered a good compromise between data fidelity and meaningful indication to ride comfort. The Griffin dataset offers lower data fidelity at high motion sickness levels, simply because the examined motions were not nausogenic enough such that only minor percentages of people reached the higher end of the Griffin motion sickness scale. The opposite is true for the low end of the motion sickness scale. Pretty much all people reached motion sickness levels 1 and 2, resulting in an abundance of 100% values in the dataset. The optimized models solve this discrepancy poorly, which is why also the models for these motion sickness levels may deliver unsatisfactory results. Nevertheless, for the sake of completeness, it was chosen to create six different motion sickness models, one for each motion sickness level defined in Table 1 respectively.

Motion sickness prediction of the original Kamiji model with unmodified parameters and the modified Kamiji model with optimized parameters plotted together with the empirical measurements of the Griffin dataset for motion sickness levels 3 and 6 are shown in Fig. 7 and Fig. 8, respectively. In these graphs, the linkage of frequency to jerk, acceleration, velocity, and displacement is chosen to be that of the Griffin dataset as dictated by the limits of the 12-m Tilting and Translating Cabin displayed in Fig. 3. This was done as it ensured that the data points of the Griffin dataset could be displayed in the same graph as the Kamiji models although these models could of course handle arbitrary motions. The parameter values for each performed optimization entailing motion sickness levels 1–6 together with the original values are given in Table 3. The highest acceleration values achieved are about 1 m/s^2 RMS at $\approx$ 0.223 Hz. Note that the original Kamiji model with parameters taken from Ref. 14, only supplies values for MSI which would correspond to motion sickness level 6. For comparative reasons, the original Kamiji model was also plotted in the plot for motion sickness level 3 shown in Fig. 7.

The performed optimization for level 3 as displayed in Fig. 7, performs well. Especially, in the case of 0% compensation which is very well covered by experiments. The fitting exhibits an inverted U-shape with a sharp peak at a constant 0.23 Hz across all compensation levels. This behavior is to be expected, as the frequency dependency of the acceleration implies that the highest acceleration amplitude is exactly at 0.23 Hz. As the output of the Kamiji model is proportional to the input magnitude, frequencies of 0.23 Hz will naturally be amplified.

The original Kamiji model exhibits much lower levels of motion sickness, which is however to be expected as the output of the original model is the percentage of people vomiting, while the model outputs the percentage of people experiencing “mild nausea.” Noticeable is the peak sensitivity of both models at around 0.23 Hz, which can be explained by the fact that the Griffin-simulator exhibits the highest input acceleration at this specific frequency. Also worth noticing is that the amplitude is increasing with increasing compensation. This effect is not confirmed by experiments. Donohew and Griffin (Ref. 11) stated that minimum motion sickness can be expected in the range of 25–50% of compensation. These findings were also experimentally confirmed by Förstberg et al. (Ref. 1), who discovered that reducing the compensation value from

Table 3. The optimized parameter vectors $\vec{p}$ of the modified Kamiji model with respect to the Griffin Motion sickness levels

Mdl	K_a	K_{ac}	K_ω	$K_{\omega c}$	K_{vc}	τ	τ_a	τ_d	K_{out}
Orig.	0.1	1.2	0.9	4	6	5	190	7	1
1	0.010139	0.11746	0.10033	0.67783	0.32642	0.96258	47.541	19.15	2.5364
2	0.010008	0.1326	0.93974	0.31455	0.27748	0.11345	175.59	17.429	1.7298
3	0.011671	1.1902	0.77774	4.9505	0.10033	0.3408	35.187	2.9101	1.2209
4	0.010815	3.2751	1.2662	5.67	5.5443	2.338	189.52	7.2055	5.9538
5	0.010075	1.5181	1.2866	0.31935	6.7999	3.839	49.578	18.538	4.3039
6	0.27879	1.6809	0.88808	5.3707	4.297	0.49003	127.58	7.4041	1.2804

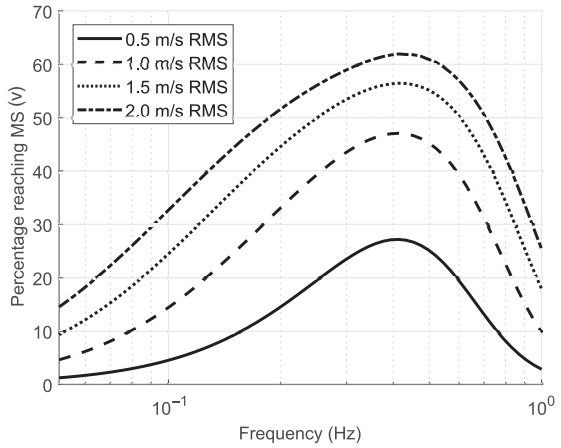

Fig. 9. Sweep of the extended Kamiji model level 6 for a compensation of 100% with fixed RMS values of acceleration.

70% to 55% reduced the symptoms of motion sickness by 25–40%. Translated to Fig. 7, this would mean that a saddle shape of the 3D plot has to be expected. Either because of insufficient fidelity of data points in the intermediate compensation ranges or because the extended Kamiji model does not offer this kind of flexibility, the model cannot reproduce these results. Some insights can be obtained by a short analysis of the optimized output parameter vector $\vec{p}$: First, the optimization algorithm reduced the parameter τ from 5 to 0.34 s, which represents the time constant of the low-pass filter estimating the "subjective vertical." Bos and Bles (Ref. 13) mentioned that this time constant was experimentally determined to be 2 s up to 20 s which is 6–60 times slower than the result of the optimization. Second, K_{out} the amplification of the MSI by the modified Kamiji model was optimized to be $K_{out} \approx 1.2$, therefore achieving the lowest values of K_{out} across all fittings. It seems that a low value of τ produces a larger conflict, which in turn leads to a lower value of K_{out}. Therefore, the algorithm has two ways to increase the output: either by decreasing τ or by increasing K_{out}. In the specific case of motion sickness level 3, the algorithm chose a lower K_{out} by decreasing τ.

In the case of Griffin-defined motion sickness level 6 as displayed in Fig. 8, the shapes are similar compared to level 3. Again the peak sensitivity of the model in this representation is 0.23 Hz because of the implicit frequency dependency of the acceleration which peaks at this frequency. A plot of the model swept over frequency with constant acceleration and 100% compensation is plotted in Fig. 9, which reveals that the peak sensitivity of the model is rather 0.43 Hz, which is higher than other research indicates (Refs. 7, 15). However, it should be noted that the Griffin dataset offers most fidelity below 0.2 Hz. As can be seen in Fig. 4, almost all motion candidates are set up below this frequency. For this reason, the optimization is not well-constrained in frequencies above 0.2 Hz which in turn leads to inaccurate modeling in this domain.

The aforementioned saddle shape also cannot be observed in Fig. 8, while an increase in MSI over compensation is again present. Whether the absence of a saddle shape has to be attributed to deficiencies in the model or rather to deficiencies in the fidelity of the Griffin dataset has yet to be determined. Again noticeable is the value of τ which at this level was optimized to be $\tau \approx 0.49$ which again leads to the conclusion that the optimization algorithm chose a relatively low K_{out} value by decreasing τ.

It should be noted that especially for very low and very high motion sickness levels, the optimization conditions are not optimal. This is evident in Fig. 8 in which especially at 0% compensation practically all data points are 0 or close to 0 which incentivizes the optimization algorithm to fit a model which outputs 0 at all times. Part of this problem is the relatively low number of test subjects reaching motion sickness level 6 during these conditions, apparently because the motion was too light to provoke satisfactory levels of motion sickness.

Conclusions

The original as well as the extended Kamiji models offers some intriguing properties over more traditional motion sickness models such as that of the ISO2631: These models can be applied to arbitrary 6-DoF motions, and they directly provide MSI data as output. Both of these properties are especially useful for various simulation, modeling, and design tasks. However, as can be seen in Fig. 7 and Fig. 8, the original Kamiji model tends to underestimate the MSI. Because short-haul vertical lift flight will mostly consist of horizontal maneuvers with some forward velocity, the Griffin dataset is a good match in order to further tune the Kamiji model, as it details motion sickness primarily for lateral oscillation with various degrees of rotational compensation which matches the foreseen flight profile of short-haul vertical lift flight motion as well as the predicted duration of these flights closely. It should be noted, however, that some drawbacks of this tuning also exist: Namely, it was tuned by applying experimental data from a motion simulator with a maximum tilt angle of 10°. Also, no outside view was given to the test subjects. It remains unclear if these testing circumstances influence the applicability to the desired field of application. However, if new data or datasets are available, it is easy to incorporate these into the optimization process. Further experimental tests will have to be conducted in order to validate and prove the developed models.

The modified Kamiji model could be optimized such that better coherence between the Griffin motion simulator tests and the model was achieved. The developed models now offer greater flexibility not only by offering more accurate predictions but also by incorporating several motion sickness levels to choose from. Using the developed simulation capability of the model, these metrics can now be easily applied in future projects for analyzing motion sickness during arbitrary motions. Especially the developed models for motion sickness levels 3 and 4 promise a good compromise between good data fidelity used as optimization input and relevant sickness levels, as at these levels motion sickness starts

to become significantly uncomfortable. These models may now be used, for example, for control design, trajectory optimization, or similar design work.

Outlook

In order to further test and validate the developed models, a set of flight-test experiments with 32 participating human test subjects onboard DLR's BO-105 helicopter has been performed. During the test flights, the passengers periodically rated their subjective motion sickness experience via the Griffin motion sickness scale. The trajectory flown during the flight test was similar to the tests performed for the Griffin dataset. In order to enable the pilot to accurately fly the required motion, an auditive cueing system was used. Data from these flight tests will enable further fine-tuning, testing, and validation of different motion sickness models, and research aimed at short-haul vertical lift transport, for example, the upcoming technology of urban air taxis. The results of these flight tests will be presented in a future publication.

References

[1]Förstberg, J., Andersson, E., and Ledin, T., "Influence of Different Conditions for Tilt Compensation on Symptoms of Motion Sickness in Tilting Trains," *Brain Research Bulletin*, Vol. 47, (5), 1998, pp. 525–535.

[2]Lawther, A., and Griffin, M. J., "Motion Sickness and Motion Characteristics of Vessels at Sea," *Ergonomics*, Vol. 31, (10), 1988, pp. 1373–1394.

[3]Vogel, H., Kohlhaas, R., and von Baumgarten, R., "Dependence of Motion Sickness in Automobiles on the Direction of Linear Acceleration," *European Journal of Applied Physiology and Occupational Physiology*, Vol. 48, (3), 1982, pp. 399–405.

[4]Turner, M., Griffin, M. J., and Holland, I., "Airsickness and Aircraft Motion during Short-Haul Flights.," *Aviation, Space, and Environmental Medicine*, Vol. 71, (12), 2000, pp. 1181–1189.

[5]Bos, J. E., MacKinnon, S. N., and Patterson, A., "Motion Sickness Symptoms in a Ship Motion Simulator: Effects of Inside, Outside, and No View," *Aviation, Space, and Environmental Medicine*, Vol. 76, (12), 2005, pp. 1111–1118.

[6]Diels, C., and Bos, J. E., "Self-Driving Carsickness," *Applied Ergonomics*, Vol. 53 Pt B, pp. 374–382, 2016.

[7]ISO Central Secretary, "ISO2631-1:1997(E) Mechanical Vibration and Shock-Evaluation of Human Exposure to Whole-Body Vibration - Part 1: General Requirements," Standard, International Organization for Standardization, Geneva, Switzerland, March 1997.

[8]Rath, T., and Fichter, W., "A closer Look at the Impact of Helicopter Vibrations on Ride Quality," in Proceedings of the AHS 73rd Annual Forum, Fort Worth, TX, , pp. 9–11, May 9–11, 2017.

[9]Joseph, J. A., and Griffin, M. J., "Motion Sickness from Combined Lateral and Roll Oscillation: Effect of Varying Phase Relationships," *Aviation, Space, and Environmental Medicine*, Vol. 78, (10), 2007, pp. 944–950.

[10]Donohew, B. E., and Griffin, M. J., "Motion Sickness with Fully Roll-Compensated Lateral Oscillation: Effect of Oscillation Frequency," *Aviation, Space, and Environmental Medicine*, Vol. 80, (2), 2009, pp. 94–101.

[11]Donohew, B. E., and Griffin, M. J., "Motion Sickness with Combined Lateral and Roll Oscillation: Effect of Percentage Compensation," *Aviation, Space, and Environmental Medicine*, Vol. 81, (1), 2010, pp. 22–29.

[12]Reason, J. T., and Brand, J. J., *Motion Sickness.* Academic Press, New York, NY, 1975.

[13] Bos, J., and Bles, W., "Modelling Motion Sickness and Subjective Vertical Mismatch Detailed for Vertical Motions," *Brain Research Bulletin*, Vol. 47, (5), 1998, pp. 537–542.

[14] Kamiji, N., Kurata, Y., Wada, T., and Doi, S., "Modeling and Validation of Carsickness Mechanism," *Proceedings of the SICE Annual Conference 2007*, IEEE, Piscataway, NJ, pp. 1138–1143, 2007.

[15]Donohew, B. E., and Griffin, M. J., "Motion Sickness: Effect of the Frequency of Lateral Oscillation," *Aviation, Space, and Environmental Medicine*, Vol. 75, (1), pp. 649–556, 2004.

[16]Beard, G. F., and Griffin, M. J., "Motion Sickness Caused by Roll-Compensated Lateral Acceleration: Effects of Centre-of-Rotation and Subject Demographics," *Proceedings of the Institution of Mechanical Engineers, Part F: Journal of Rail and Rapid Transit*, Vol. 228, (1), 2014, pp. 16–24.

[17]O'Hanlon, J. F. O., and McCauley, M. E., "Motion Sickness Incidence as a Function of the Frequency and Acceleration of Vertical Sinusoidal Motion," *Aviation, Space, and Environmental Medicine*, Vol. 45, pp. 366–369, 1974.